Chapter 3

Characteristic, dynamic and near saturation regions of Out-of-time-order correlation in Floquet Ising models

3.1 Introduction

Larkin and Ovchinnikov first introduced the concept of out-of-time-order correlation (OTOC) for defining approaches from quasi-classical to quantum systems [19]. In recent years OTOCs have gotten attention in various fields [14, 20, 21, 22, 23, 24, 25, 26, 26, 27, 124] such as quantum chaos and information propagation in quantum many-body systems [9, 10, 97, 99, 125, 126, 127], quantum entanglement and quantum-information delocalization [12, 14, 58, 128, 129, 130, 131], static and dynamical phase transitions [25, 50, 132]. Several proposals for experimental measurement of OTOC are proposed [16, 17, 18, 133, 134] using cold atoms or cavity and circuit quantum electrodynamics (QED) or trapped-ion simulations. Experimental realisations have been made using nuclear spins of molecules [101, 128, 132], trapped ions [135, 136], and ultra-cold gases [137]. Chaotic characteristics of OTOC are manifested if a small disturbance in the input of the

system provides exponential deviation to the output of the system, which is known as butterfly effect [8, 9].

Classical Hamiltonian systems, which have highest amount of randomness and chaos, are converted into the quantum domain for seeing the behavior of quantum chaos [23, 124]. OTOC finds a role in characterizing the quantum chaos in these systems. There exist a characteristic form of growth of OTOC that can distinguish different classes of information scrambling. In a chaotic case, OTOC grows very fast, which is often described by an exponential behavior with a Lyapunov exponent. If the chaos is absent, the growth of OTOC can be much slower or even absent. In disordered systems, OTOC distinguishes many-body localization [138, 139, 140] from the Anderson localization [141].

Growth of OTOC is also discussed in spin systems [58, 59, 60, 61, 62, 63, 64, 65, 66, 67, 68, 69]. Power-law growth of OTOC is observed in the dynamic region of Luttinger liquid model [67], XY model [66], integrable quantum Ising chain [58] and some systems exhibiting many-body localization [68, 69]. Similar studies have been done in the Ising model with tilted magnetic fields, perturbed XXZ model, and Heisenberg spin chain with random magnetic fields [62]. In these systems, OTOC is calculated for different types of observables. For the observables that are local, non-local or mixed in terms of the Jordon-Wigner (JW) fermions, the OTOCs grow as power-law in time [58].

The quantum systems periodically driven by external forces received considerable attention for a long time. Examples are: kicked-rotor model in which a particle moving on a ring and field is applied in the form of kicks [142], Chirikov standard map [143], and the Kapitza pendulum [144]. These systems show a transition from integrability to chaos, dynamical localization [145, 146], and dynamical stabilization [144, 147]. In recent years, in the quantum domain such as time crystal [148, 149], the topological system with ultra-cold atoms [150, 151], a periodically-driven quantum system such as particle moving in a modulated harmonic trap [152], kicked quantum rotors [153, 154, 155],

Floquet spin systems with constant fields [25, 53, 54, 55, 156, 157] and quenched fields [158, 159, 160, 161, 162] got considerable attention. Periodic perturbation can be realized in experiments to understand specific properties of matter [153, 163, 164, 165]. OTOC generated by the sum of quadratic and composite observables in terms of Majorana fermions is studied in integrable and nonintegrable kicked quantum Ising system [61] shows linear growth with time and starts to saturate at $t \simeq N/2$, where, N is the system size. OTOCs using local and nonlocal observables for Floquet XY and synchronized Floquet XY models are also studied recently [166]. In our previous study [25], we could get the phase structure using time-averaged longitudinal magnetization OTOC (LMOTOC), but transverse magnetization OTOC (TMOTOC) failed to give us the phase diagram. While thoroughly understanding the comparison between the initial and the time-averaged behavior of integrable TMOTOC and LMOTOC, we found the different characteristic times. In this chapter, we carry out a comprehensive study of the entire region of OTOC in the integrable as well as nonintegrable Floquet spin models, not just the initial time or averaged behavior. We will analyze whether the integrability breaking term changes the growth of OTOC. We extract the differences and similarities of TMOTOC and LMOTOC for integrable and nonintegrable models.

This chapter is structured as follows: In section 3.2, we will discuss the Floquet transverse Ising models. Subsequently, in section 3.3, we will define transverse magnetization OTOC (TMOTOC) and longitudinal magnetization OTOC (LMOTOC). Later, we discuss results in section 3.4 while comparing the calculations of integrable and nonintegrable Floquet transverse Ising models in both TMOTOC and LMOTOC. Finally, we conclude the results in section 3.5.

3.2 Model

Consider a periodically driven interacting transverse Ising Floquet system. The Hamiltonian of the system is given as

$$\hat{H}(t) = J_x \hat{H}_{xx} + h_z \sum_{n=-\infty}^{\infty} \delta\Big(n - \frac{t}{\tau}\Big)\hat{H}_z, \tag{3.1}$$

where J_x is the nearest-neighbor exchange coupling strength, and h_z is the external field in the transverse direction applied in the form of kicks at equal intervals of time τ. $\hat{H}_{xx} = \sum_{l=1}^{N} \hat{\sigma}_x^l \hat{\sigma}_x^{l+1}$ is the nearest-neighbor Ising interaction term and $\hat{H}_z = \sum_{l=1}^{N} \hat{\sigma}_z^l$ is the interaction of unit magnetic field with the total transverse magnetization.

Floquet map corresponding to the Eq. (3.1) is

$$\hat{\mathscr{U}}_0 = \exp(-i\tau J_x \hat{H}_{xx}) \exp(-i\tau h_z \hat{H}_z), \tag{3.2}$$

Since in Eq. (3.1) there is only transverse field is present, and the Hamiltonian is exactly solvable using Jordan-Wigner (JW) transformation [54, 167, 168]. Now, if we introduce a longitudinal field term $h_x \hat{H}_x = h_x \sum_{l=1}^{N} \hat{\sigma}_x^l$, the Hamiltonian can be written as

$$\hat{H}(t) = J_x \hat{H}_{xx} + h_x \hat{H}_x + h_z \sum_{n=-\infty}^{\infty} \delta\Big(n - \frac{t}{\tau}\Big)\hat{H}_z. \tag{3.3}$$

However, the model could not be transformed into the free fermions using JW transformation because the longitudinal field term, when transformed into JW fermions, gives an interacting fermionic term [167, 168]. The Floquet map corresponding to this model is

$$\hat{\mathscr{U}}_x = \exp\big[-i\tau(J_x \hat{H}_{xx} + h_x \hat{H}_x)\big] \exp(-i\tau h_z \hat{H}_z). \tag{3.4}$$

Henceforth in the chapter, we mean integrable transverse Ising Floquet model as $\hat{\mathscr{U}}_0$ and nonintegrable transverse Ising Floquet model as $\hat{\mathscr{U}}_x$.

3.3 TMOTOC and LMOTOC

Let us consider a pair of observables $\hat{W}^l$ and $\hat{V}^m$ at l^{th} and m^{th} sites, respectively. OTOC of these observables is defined as

$$C^{l,m}(n) = -\frac{1}{2}\langle[\hat{W}^l(n),\hat{V}^m(0)]^\dagger[\hat{W}^l(n),\hat{V}^m(0)]\rangle. \tag{3.5}$$

Observables, $\hat{W}^l$ and $\hat{V}^m$ are separated by distance $\Delta l = |l-m|$. Initially at $n = 0$, both the observables commute to each other, *i.e.* $[\hat{W}^l(0),\hat{V}^m(0)] = 0$. As time increases, higher order terms of the time evolution of $\hat{W}^l(0)$ given by the Baker-Campbell-Hausdorff formula fail to commute with $\hat{V}^m$, resulting in noncommutative $\hat{W}^l(n)$ and $\hat{V}^m$. By examining the noncommutativity of $\hat{V}^m$ at different positions, one can quantify upto some degree how $\hat{W}^l(n)$ spread over the space. Here $\hat{W}^l(n)$ is $(\hat{\mathscr{U}}_{x/0}^\dagger)^n\hat{W}^l(0)(\hat{\mathscr{U}}_{x/0})^n$. If $\hat{W}^l$ and $\hat{V}^m$ are Hermitian and unitary, the OTOC simplifies in the form

$$C^{l,m}(n) = 1 - \Re[F^{l,m}(n)], \tag{3.6}$$

where, $F^{l,m}(n) = \langle\hat{W}^l(n)\hat{V}^m(0)\hat{W}^l(n)\hat{V}^m(0)\rangle$ and $\langle\cdot\rangle$, denotes the quantum mechanical average over the initial state.

OTOC is calculated with either trace over a maximally mixed state or a thermal ensemble. Trace can be replaced by employing Haar random states of 2^N dimensions to evaluate expectation values, that is

$$\text{Tr}(\hat{W}^l(n)\hat{V}^m(0)\hat{W}^l(n)\hat{V}^m(0))/2^N \approx \left\langle\Psi_R\middle|\hat{W}^l(n)\hat{V}^m(0)\hat{W}^l(n)\hat{V}^m(0)\middle|\Psi_R\right\rangle \tag{3.7}$$

where $|\Psi_R\rangle$ is a random state. We replaced the random state by two fully polarized special initial states according to the observables and found that there are no remarkable differences in the characteristic, dynamic, and saturation regions of OTOC. We observe only one difference in the saturation region, and there are comparatively small oscillations when considering a random state. Detailed discussion is mentioned in Appendix B-I. Moreover, the special initial states may help to get the exact analytical formula, at least for integrable OTOC cases with transverse direction spins as observables.

In this chapter, we consider $\hat{W}^l$ and $\hat{V}^m$ as local Pauli operators either in the longitudinal direction $\hat{\sigma}_x^{l,m}$ or in the transverse direction $\hat{\sigma}_z^{l,m}$. For the Pauli operators in the transverse direction as local observables, the OTOC is defined as transverse magnetization OTOC (TMOTOC) and given as:

$$C_z^{l,m}(n) = 1 - \Re[F_z^{l,m}(n)], \tag{3.8}$$

where, $F_z^{l,m}(n) = \langle\phi_0|\hat{\sigma}_z^l(n)\hat{\sigma}_z^m\hat{\sigma}_z^l(n)\hat{\sigma}_z^m|\phi_0\rangle$. In the fermionic representation, $\hat{\sigma}_z^l$ can be written as $\hat{\sigma}_z^l = -(\prod_{j<l}A^jB^j)A^l$, where, A^l and B^l are defined by fermionic creation ($c^{l\dagger}$) and annihilation operator (c^l) as, $A^l = c^{l\dagger} + c^l$ and $B^l = c^{l\dagger} - c^l$ [169]. Since $\hat{\sigma}_z^l$ contain string operator, hence it is known as non-local operator in terms of Jordan-Wigner fermion [58, 169].

For the calculation purpose we take initial state as $|\phi_0\rangle = |\uparrow\uparrow\uparrow\cdots\uparrow\rangle$, where $|\uparrow\rangle$ is the eigenstate of $\hat{\sigma}_z$ with eigenvalue $+1$. If the observables are taken as Pauli operators in the longitudinal direction of the Ising axis (*i. e.,* z-axis), then OTOC will be referred to as longitudinal magnetization OTOC (LMOTOC). The LMOTOC is given as follows:

$$C_x^{l,m}(n) = 1 - \Re[F_x^{l,m}(n)], \tag{3.9}$$

where, $F_x^{l,m}(n) = \langle\psi_0|\hat{\sigma}_x^l(n)\hat{\sigma}_x^m\hat{\sigma}_x^l(n)\hat{\sigma}_x^m|\psi_0\rangle$. In the fermionic representation, $\hat{\sigma}_x^{l/m}$ can be written as $\hat{\sigma}_x^{l/m} = A^{l/m}B^{l/m}$. In fermionic representation $\hat{\sigma}_x^{l/m}$ is known as local observable

[58, 169]. In this case the initial state will be taken as $|\psi_0\rangle = |\rightarrow\rightarrow\rightarrow\cdots\rightarrow\rangle$, where, $|\rightarrow\rangle$ is the eigenstate of $\hat{\sigma}_x$ with eigenvalue $+1$.

3.3.1 Analytical formula of TMOTOC

Analytical solution of the TMOTOC for the initial state $|\phi_0\rangle = |\uparrow\uparrow\uparrow\cdots\uparrow\rangle$ and Floque map defined by Eq. (3.2) with $J_x = 1$ and $h_z = 1$ is derived in the Ref. [25] as

$$\begin{aligned} F_z^{l,m}(n) &= 1 - \Big(\frac{2}{N}\Big)^3 \sum_{p,q,r} \Big[e^{i(p-q)(m-l)} |\Psi_r(n)|^2 \Phi_p^*(n)\Phi_q(n) \\ &- e^{i(-r-q)(m-l)} \Psi_r(n)^* \Phi_p^*(n)\Phi_q(n)\Psi_{-p}(n) \\ &- e^{i(p+q)(m-l)} \Psi_q(n)\Psi_r(n)^*\Phi_p(n)^*\Phi_{-r}(n) \\ &+ e^{i(q-r)(m-l)} \Psi_q(n)\Psi_r(n)^* |\Phi_p(n)|^2 \Big], \end{aligned} \tag{3.10}$$

where the expansion coefficients $\Phi_q(n)$ and $\Psi_q(n)$ are defined as

$$\Phi_q(n) = |\alpha_+(q)|^2 e^{-in\gamma_q} + |\alpha_-(q)|^2 e^{in\gamma_q}, \tag{3.11}$$

$$\Psi_q(n) = \alpha_+(q)\beta_+(q)e^{-in\gamma_q} + \alpha_-(q)\beta_-(q)e^{in\gamma_q}. \tag{3.12}$$

The phase angle γ_q and the coefficients $\alpha_\pm(q)$ and $\beta_\pm(q)$ are given by

$$\cos(\gamma_q) = \cos(2\tau)\cos(4\tau) - \cos(q)\sin(2\tau)\sin\Big(2\tau\Big), \tag{3.13}$$

and

$$\alpha_\pm(q)^{-1} = \sqrt{1 + \Big(\frac{\cos(2\tau) - cos(\gamma_q \pm 2\tau)}{\sin(q)\sin(2\tau)\sin(2\tau)}\Big)^2}, \tag{3.14}$$

$$\beta_{\pm}(q) = \frac{\mp\sin(\gamma_q) - \cos(2\tau)\sin(2\tau)\big(\cos(q)+1\big)}{\sin(q)\sin(2\tau)}\alpha_{\pm}(q)e^{-i2\tau}. \tag{3.15}$$

The allowed value of p, q and r are from $\frac{-(N-1)\pi}{N}$ to $\frac{(N-1)\pi}{N}$ differing by $\frac{2\pi}{N}$ for even number of N_F ($N_F = \sum_l c_l^\dagger c_l$, number of fermions) and $\hbar = 1$. We use the above exact solution to calculate TMOTOC for integrable $\hat{\mathscr{U}}_0$ model. However, TMOTOC for the nonintegrable $\hat{\mathscr{U}}_x$ model, and LMOTOC for both integrable $\hat{\mathscr{U}}_0$ and nonintegrable $\hat{\mathscr{U}}_x$ model will be calculated numerically.

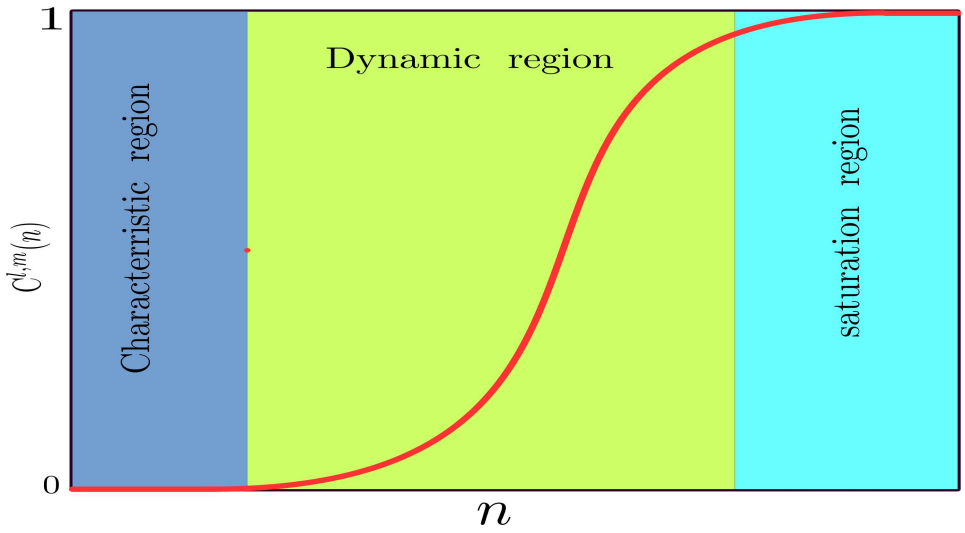

Fig. 3.1 Schematic of the various regions of OTOC in a typical system.

3.4 Results

We analyze TMOTOC and LMOTOC for both $\hat{\mathscr{U}}_0$ and $\hat{\mathscr{U}}_x$ models in three regions as depicted in the Fig. 3.1. These are, namely:

i) *Characteristic Region:* Both the observables $\hat{W}^l$ and $\hat{V}^m$ commute with each other till the characteristic time ($t_{\Delta l}$), which is defined as time after that $C^{l,m}_{z/x}(n)(F^{l,m}_{z/x}(n))$

is departed from zero (one). The Characteristic time depends upon the separation between the spins ($\Delta l = |l-m|$). As we increase the separation between the spins, the characteristic time increases, and it is independent of the Floquet period and system size.

ii) *Dynamic Region:* After the characteristic time, $C^{l,m}_{z/x}(n)$ becomes nonzero. In the dynamic region $C^{l,m}_{z/x}(n)$ increases rapidly.

iii) *Near saturation Region:* After rapid growth, $C^{l,m}_{z/x}(n)$ starts to saturate to a finite value. However, the manner in which $C^{l,m}_{z/x}(n)$ saturates follows some trend with an oscillating amplitude. Such trend we calculate by analysing behaviour of $\Re[F^{l,m}_{z/x}(n)]$ vs. n.

3.4.1 TMOTOC in the integrable Floquet system

Let us begin with TMOTOC for integrable $\hat{\mathscr{U}}_0$ system defined by Eq. (3.2). First, we focus on the characteristic region of TMOTOC with increasing Floquet period. Let us consider an operator $\hat{W}$ located at site l initially. One can see that the considered Floquet evolution increases the size of $\hat{W}$ at each Floquet step. In particular, the left end of the support of $\hat{W}(n)$ and the right end of the support of $\hat{W}(n)$ will increase by one for each Floquet step. We, therefore, can see that $\Re[F^{l,m}_z(n)] = 1$ if $n < |l-m|$. However, once $n \geq |l-m|$, $\Re[F^{l,m}_z(n)]$ will start to deviate from 1.

Fig. 3.2(a) is the behaviour of $\Re[F^{l,m}_z(n)]$ with increasing Floquet period and fixed $\Delta l = 6$. One can see from Fig. 3.2(a) that $\Re[F^{l,m}_z(n)]$ start to deviate at $\Delta l^{\text{th}} (= 6^{\text{th}})$ kick for all Floquet period (τ). This characteristic time is independent of the Floquet period and system size (N) (we have checked till $N = 50$). For a fixed Floquet period τ, we can see the behavior of $\Re[F^{l,m}_z(n)]$ with the number of kicks and see the dependence of $t_{\Delta l}$ on Δl. In Fig. 3.2(b), for $\tau = \frac{6\epsilon}{2}$, we show $\Re[F^{l,m}_z(n)]$ vs. the number of kicks by changing

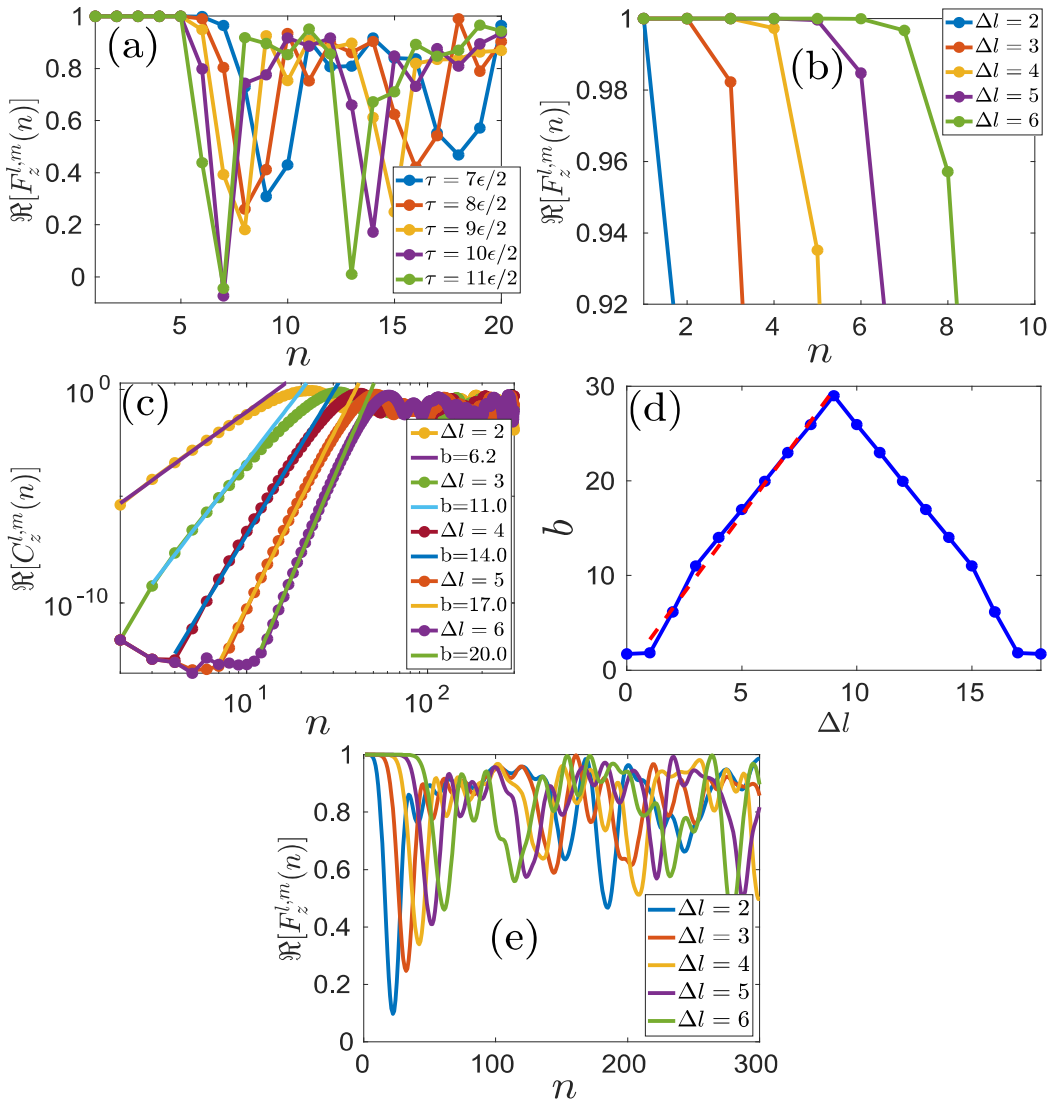

Fig. 3.2 Integrable transverse Ising Floquet system with $J_x = 1$ and $h_z = 1$ for $N = 18$. (a) The behavior of $TMOTOC$ with the number of kicks (n) by increasing the value of Floquet period from $\frac{7\varepsilon}{2}$ to $\frac{11\varepsilon}{2}$ differing by $\varepsilon/2$ with fixed $\Delta l = 6$ ($\varepsilon = \frac{\pi}{28}$). (b) $F_z^{l,m}$ with number of kicks by increasing Δl and fixed Floquet period $\tau = 6\varepsilon/2$. (c) $C_z^{l,m}$ with number of kicks (log − log) with increasing distances (Δl) between the spins at constant Floquet period $\tau = \frac{\varepsilon}{2}$. (d) Exponent of power-law with increasing distance between the spins. (e) $\Re[F_z^{l,m}]$ with number of kicks at different Δl.

the separation between the observables $\Delta l = |l - m|$. We see that increasing the separation between the spins, increases the characteristic time for the TMOTOC case, and number of kicks required to deviate from unity is equal to the separation between the observables ($n = \Delta l$). The growth of TMOTOC in the dynamic region follows a power-law. The exponent of the power-law increases with increasing the separation between the local spin observables in a systematic manner [Fig. 3.2(c)]. The exponent increases, reaches the maximum at $\Delta l = \frac{N}{2}$, and further decreases with increasing the distance between the spins [Fig. 3.2(d)]. The exponent of the power-law can be expressed as a triangular function:

$$b \approx b_{\max} - \kappa \left| \frac{N}{2} - \Delta l \right|, \qquad 1 \leq \Delta l \leq N - 1. \tag{3.16}$$

where, the constants $\kappa = 3.2$, $b_{\max} = 29$ and $b_0 = 1.7$. Eq. (3.16) shows the dependence of the exponent of power-law with increasing the separation between the observables. It is symmetric about $\Delta l = \frac{N}{2}$ because of the periodic boundary condition of the spin chains. $\Re[F_z^{l,m}(n)]$ revives back to unity after a few kicks in the saturation region. Revival time has nontrivial dependence on n and Δl [Fig. 3.2(e)]. The TMOTOC extracted from the analytical expression Eq. (2.6) in characteristic, dynamic, and saturation regions can be summarised as

$$C_z^{l,m}(n) \approx \begin{cases} 0, & n\tau < t_{\Delta l}, \\ (n\tau)^{\kappa \Delta l + 2}, & t_{\Delta l} < n\tau < t_s, \\ \text{revived} \quad \text{back}, & t_s < n\tau. \end{cases} \tag{3.17}$$

In the above expression, $t_{\Delta l}$ is characteristic time, and t_s is the time at which TMOTOC starts saturating. Dynamic region of TMOTOC decreases with increasing the Floquet period τ as shown in Fig 3.3(a-e). In general the dependence on τ is such that we can define $C_z^{l,m} \propto (n\tau)^{\kappa \Delta l + 2}$ in dynamic region.

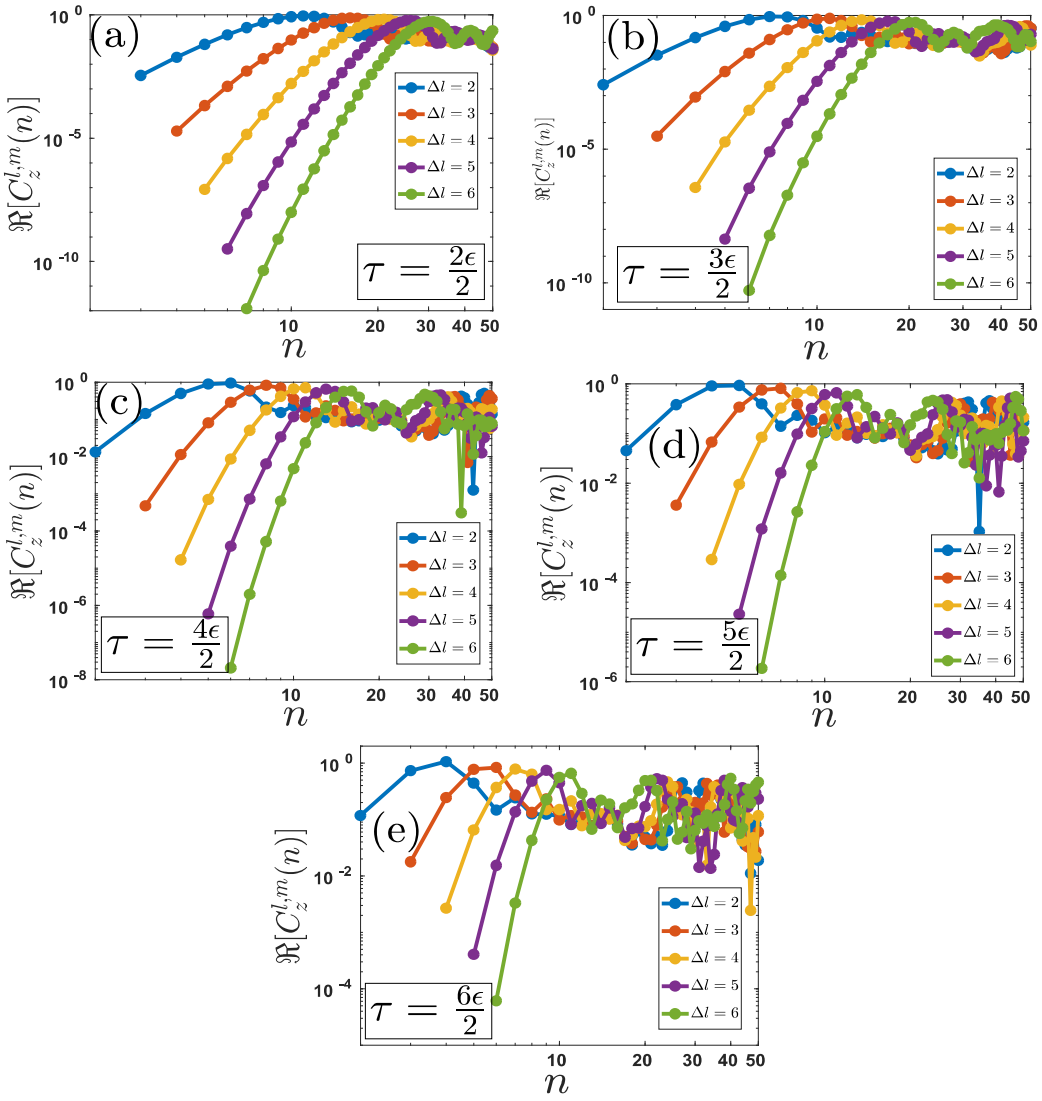

Fig. 3.3 Integrable transverse Ising Floquet system with $J_x = 1$ and $h_z = 1$ for $N = 18$. Behaviour of $TMOTOC$ with number of kicks (n) by increasing Δl from 2 to 6 at different Floquet period (a) $\tau = \frac{2\varepsilon}{2}$, (b) $\tau = \frac{3\varepsilon}{2}$, (c) $\tau = \frac{4\varepsilon}{2}$, (d) $\tau = \frac{5\varepsilon}{2}$ and (e) $\tau = \frac{6\varepsilon}{2}$ ($\varepsilon = \frac{\pi}{28}$)

.

3.4.2 TMOTOC in the nonintegrable Floquet system

Now, we use the nonintegrable $\hat{\mathscr{U}}_x$ model given by Eq. (3.4) and analyze the TMOTOC. Fig. 3.4(a) shows the behavior of $\Re[F_z^{l,m}(n)]$ for varying τ and fixed $\Delta l = 6$. From Fig. 3.4(a), one can see that number of kicks required for $\Re[F_z^{l,m}(n)]$ depart from unity is equal to the separation between the observables ($n = |l-m|$). Hence characteristic time does not depend on the Floquet periods. Let us explore the behavior of TMOTOC with the distance between the spins for a fixed τ (say $\tau = \frac{6\varepsilon}{2}$) and increase the separation between the spins Δl. As Δl increases, the characteristic time $(t_{\Delta l})$ increases in such a way that $n = \Delta l$ [Fig. 3.4(b)]. Dynamic region of TMOTOC for the nonintegrable is again showing power-law, and the exponent of the power-law (b) depends on Δl [Fig. 3.4(c)]. b increases with increasing Δl and reaches a maximum $(b_{\max})$ at $\Delta l = \frac{N}{2}$ and afterwards decreases symmetrically with increasing Δl before coming down to b_1 at $\Delta l = N-1$. Since we consider the periodic boundary condition, the exponent of the power-law is symmetric about $\Delta l = \frac{N}{2}$ [Fig. 3.4(d)]. In a mathematical form we can express b, approximately, by Eq. (3.16) with $\kappa = 3.2$, $b_{\max} = 28$ and $b_{\min} = 1.78$. Saturation of $\Re[F_z^{l,m}(n)]$ in this nonintegrable model is following a linear decaying behavior with a very small slope for all Δl [Fig. 3.4(e)]. TMOTOC for $\hat{\mathscr{U}}_x$ model in all the regions is summed up as

$$C_z^{l,m}(n) \approx \begin{cases} 0, & n\tau < t_{\Delta l}, \\ (n\tau)^{\kappa\Delta l+1}, & t_{\Delta l} < n\tau < t_s, \\ 1-\mu n, & t_s < n\tau. \end{cases} \tag{3.18}$$

where $\mu = 0.002$ and $\kappa = 3.2$. We calculate the exponent of the power-law by using the HBC formula for $\Delta l = 1, 2$ and find approximate matches with the exponent of the power-law in the dynamic region of Eq. (3.18). Detailed calculation is given in the Appendix B-II.

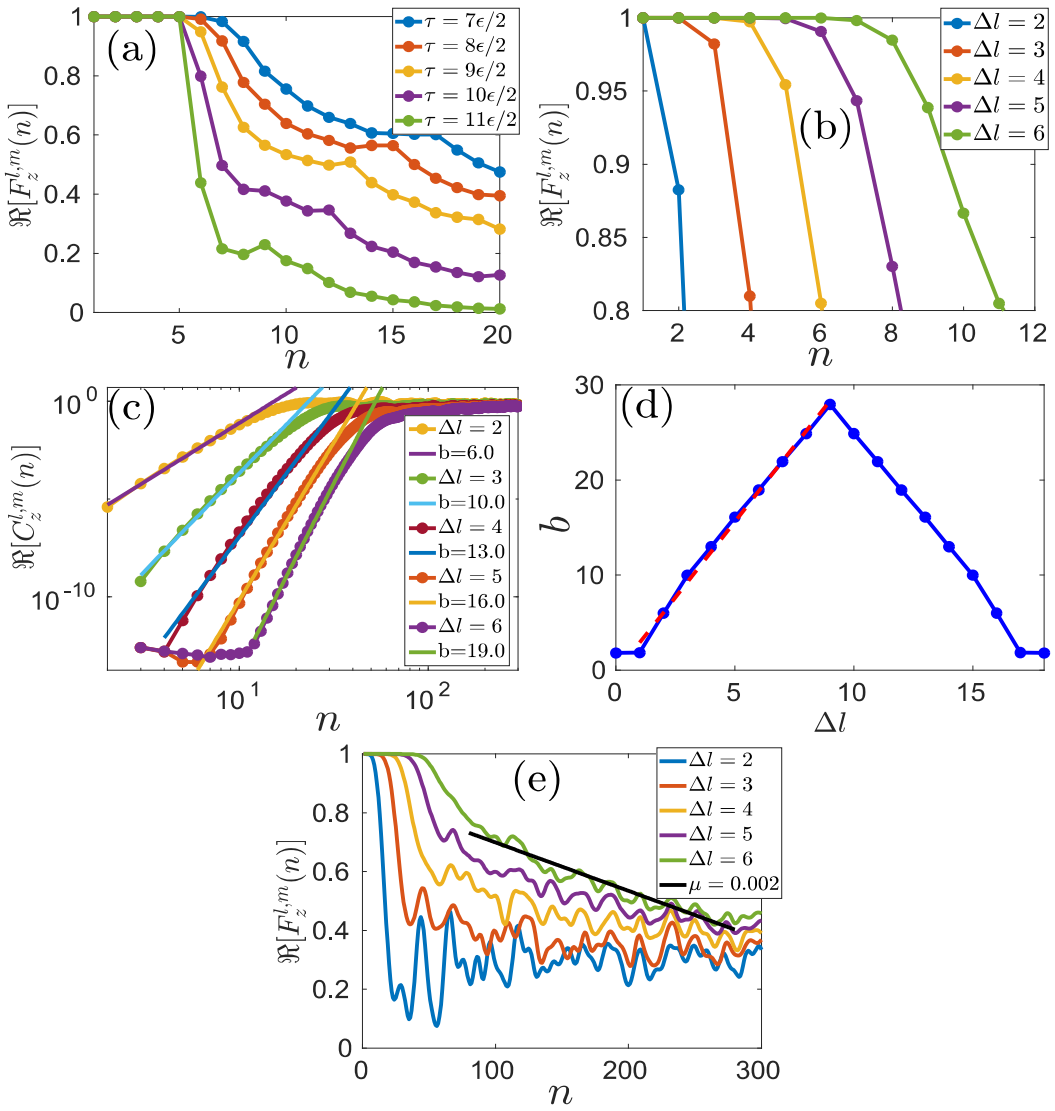

Fig. 3.4 Non-integrable closed chain transverse Ising Floquet system with $J_x = 1$, $h_z = 1$, and $h_x = 1$ of size $N = 18$. (a) Behavior of $TMOTOC$ with number of kicks (n) by increasing value of Floquet period from $\frac{7\varepsilon}{2}$ to $\frac{11\varepsilon}{2}$ differing by $\frac{\varepsilon}{2}$ with fixed $\Delta l = 6$ ($\varepsilon = \frac{\pi}{28}$). (b) Initial region of $F_z^{l,m}$ with number of kicks with increasing distances between the spins (Δl) and fixed Floquet period $\tau = 6\varepsilon/2$. (c) $C_z^{l,m}$ with number of kicks $(\log - \log)$ with increasing (Δl) at fixed $\tau = \frac{\varepsilon}{2}$. (d) Changing of power with Δl. (e) Saturation of $F_z^{l,m}$ with the number of kicks.

3.4.3 LMOTOC in the integrable Floquet system

Now we focus on the LMOTOC for the integrable $\hat{\mathscr{U}}_0$ model which shows a similarity with TMOTOC for the same model. Fig. 3.5(a) is the behavior of LMOTOC at different Floqeut periods and fixed $\Delta l = 6$. In the LMOTOC, number of kicks required to deviate from unity is $n = \Delta l + 1$. In comparison with TMOTOC, LMOTOC required one more kick to deviate $\Re[F_x^{l,m}(n)]$ from unity because $\hat{\sigma}_x^l$ (using Baker–Campbell–Hausdorff formula) provides spreading terms after the first kick. Hence, characteristic time does not depend on the Floquet period, however, it depends on the separation between the observables in such a way that characteristic time increases linearly with increasing the separation between the observables ($n = \Delta l + 1$) [Fig. 3.5(b)]. In the dynamic region of LMOTOC at a small Floquet period, we get a power-law behavior similar to the TMOTOC case. The exponent of the power-law increase with Δl in the same manner as in the TMOTOC case [Fig. 3.5(c)]. We can approximate the exponent with Δl by Eq. (3.16) with $\kappa = 3.4$, $b_{\max} = 32.9$ and $b_0 = 1.9$ [Fig. 3.5(d)]. Saturation region of LMOTOC for $\hat{\mathscr{U}}_0$ shows oscillating behavior. The envelope of the oscillation decays linearly with a constant slope for all Δl [Fig. 3.5(e)]. This behavior is a contrast to the saturation region of TMOTOC for $\hat{\mathscr{U}}_0$ which displays a revival to early-time behavior. All the regions of LMOTOC for $\hat{\mathscr{U}}_0$ can be encapsulated as

$$C_x^{l,m}(n) \approx \begin{cases} 0, & n\tau < t_{\Delta l}, \\ (n\tau)^{\kappa\Delta l+6}, & t_{\Delta l} < n\tau < t_s, \\ 1-\mu n, & t_s < n\tau. \end{cases} \tag{3.19}$$

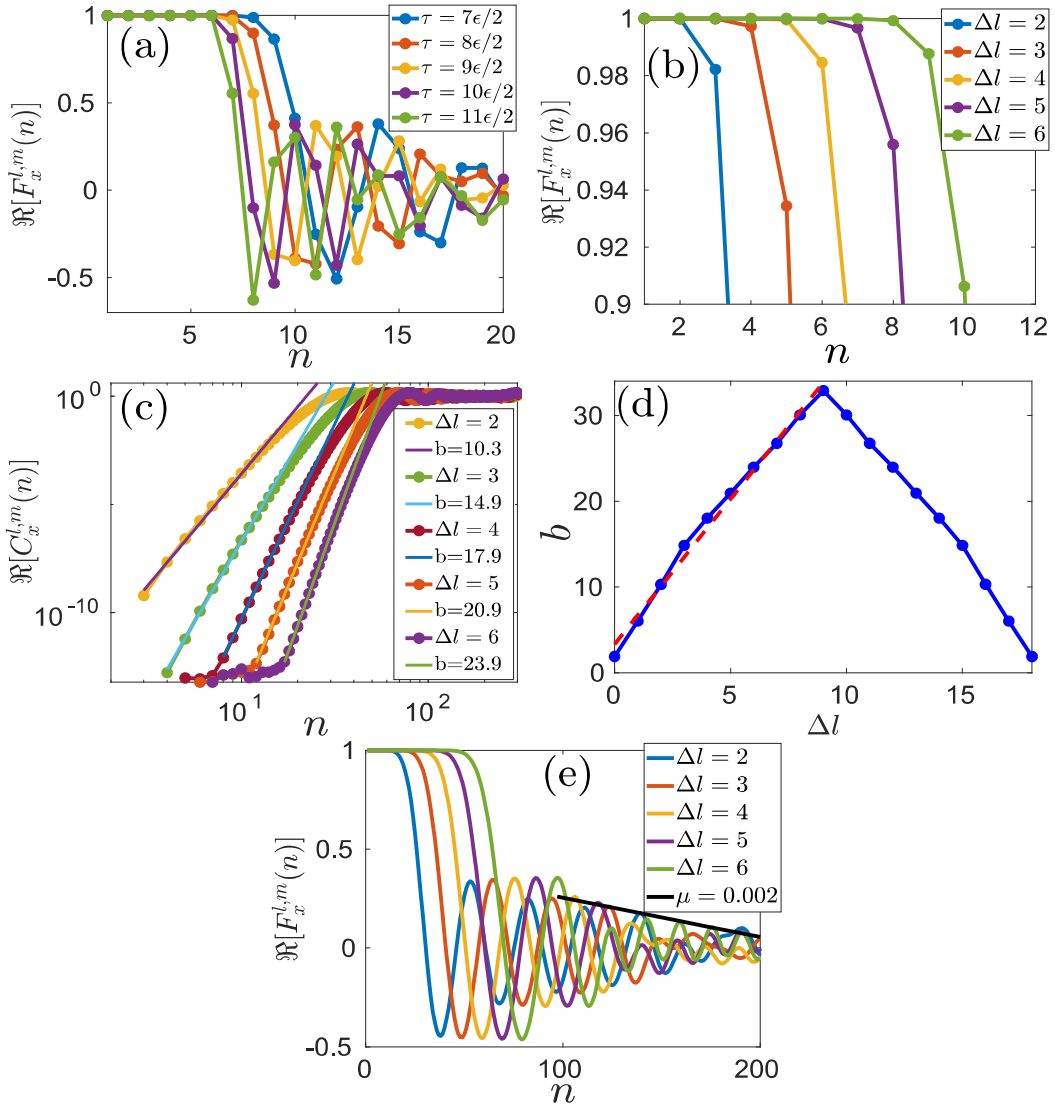

Fig. 3.5 Integrable closed chain transverse Ising Floquet system with $J_x = 1$ and $h_z = 1$ of size $N = 18$. (a) Behaviour of *LMOTOC* with number of kicks (n) with increasing value of Floquet periods from $\frac{7\varepsilon}{2}$ to $\frac{11\varepsilon}{2}$ differing by $\frac{\varepsilon}{2}$ and $\Delta l = 6$ ($\varepsilon = \frac{\pi}{28}$). (b) $F_x^{l,m}(n)$ with number of kicks with increasing (Δl) and fixed Floquet period $\tau = 6\varepsilon/2$. (c) $C_x^{l,m}(n)$ with number of kicks $(\log - \log)$ with increasing Δl at fixed $\frac{\varepsilon}{2}$. (d) Changing of power with Δl. (e) $F_x^{l,m}(n)$ with number of kicks at different Δl. Black line represents the exponential decreasing of maxima of saturation amplitude.

3.4.4 LMOTOC in the nonintegrable Floquet system

Finally, we consider nonintegrable $\hat{\mathscr{U}}_x$ model for LMOTOC calculations. We get similar behavior in the characteristic regime as that for LMOTOC with $\hat{\mathscr{U}}_0$ model [Fig. 3.6(a) and (b)]. In the dynamic region, the growth is again a power-law, and the exponent increase with Δl [Fig. 3.6(c)] but the trend is a bit different than the previous cases. Unlike the previous cases, we see a quadratic increase of the exponent by increasing Δl, till a maximum is reached. After the maximum $b_{\max}$ at $\Delta l = \frac{N}{2}$, we see a symmetric decrease in the exponent till $\Delta l = N$ [Fig. 3.6(d)]. We approximate b as follows:

$$b \approx \left(b_{\max} - \lambda \left|\frac{N}{2} - \Delta l\right|^2\right). \qquad 0 \leq \Delta l \leq N \tag{3.20}$$

Where $\lambda = 2.8$, $b_{\max} = 24.0$ and $b_0 = 1.7$. Eq. (3.20) describes the variation of exponent of power-law with increasing the separation between the observables. It is a parabolic form with vertex at $\frac{N}{2}$ and also symmetric about $\Delta l = \frac{N}{2}$ because of closed chain consideration. We calculate the exponent of the power-law by using the HBC formula for $\Delta l = 1$ and find that exponent approximately matches the Eq. (3.20). Detailed calculation is mentioned in Appendix B-III. Saturation of LMOTOC for a nonintegrable case is oscillating, and the maxima of the oscillation decrease linearly (with a very small slope $\mu = 10^{-5}$, and same for all Δl) with the number of kicks [Fig. 3.6(e)]. The complete region of LMOTOC for $\hat{\mathscr{U}}_x$ system is given as

$$C_x^{l,m}(n) \approx \begin{cases} 0, & n\tau < t_{\Delta l}, \\ (n\tau)^{\lambda(\Delta l)^2}, & t_{\Delta l} < n\tau < t_s, \\ 1 - \mu n, & t_s < n\tau. \end{cases} \tag{3.21}$$

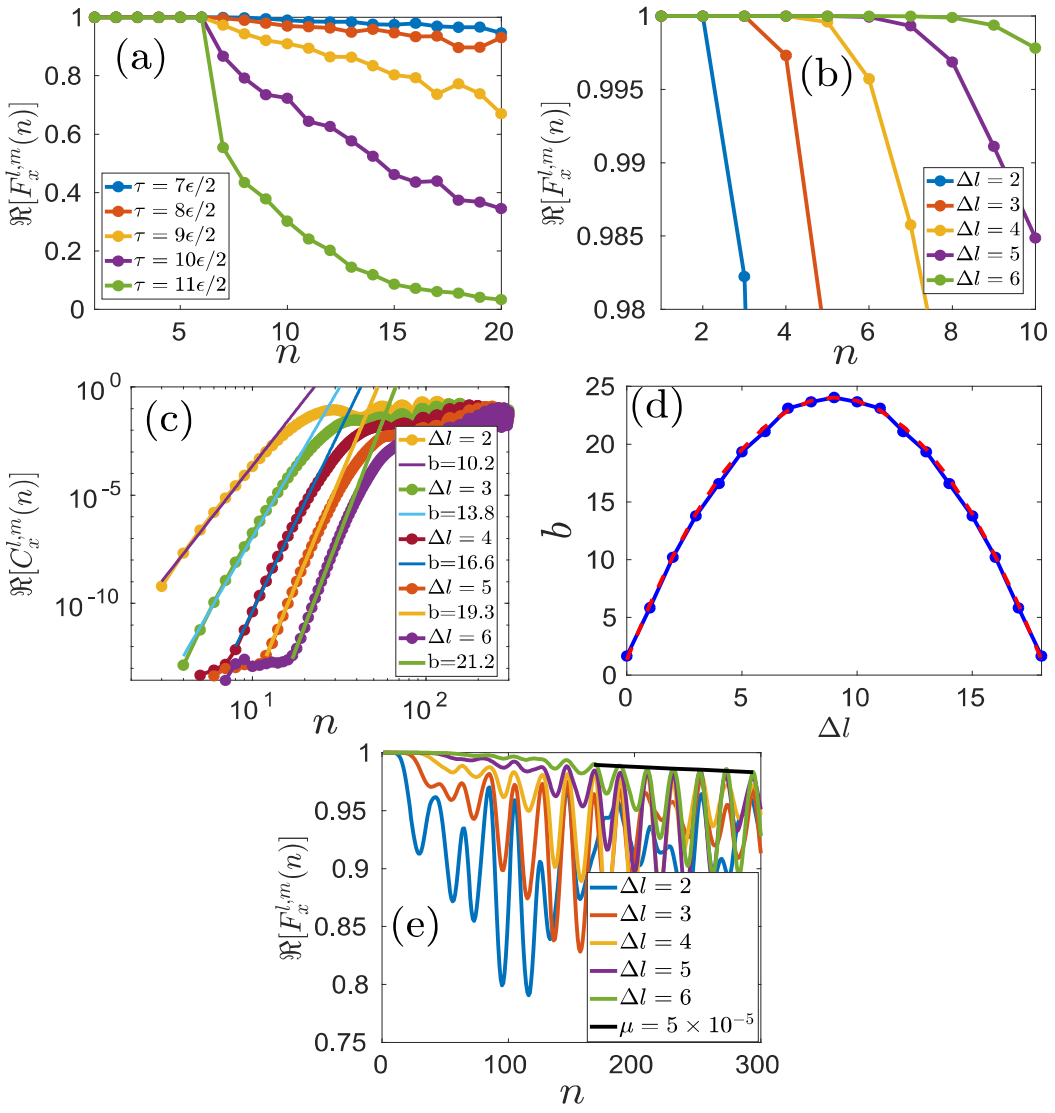

Fig. 3.6 Non-integrable closed chain transverse Ising Floquet system with $J_x = 1$, $h_z = 1$, and $h_x = 1$ for $N = 18$. (a) *LMOTOC* with number of kicks (n) by increasing value of Floquet period from $\frac{7\varepsilon}{2}$ to $\frac{11\varepsilon}{2}$ differing by $\frac{\varepsilon}{2}$ with fixed $\Delta l = 6$ ($\varepsilon = \frac{\pi}{28}$). (b) $F_x^{l,m}(n)$ with increasing Δl from 6 to 6 and fixed period $\tau = \frac{6\varepsilon}{2}$. (c) $C_x^{l,m}(n)$ with number of kicks (log − log) by increasing Δl from 2 to 6 and fixed Floquet period $\tau = \frac{\varepsilon}{2}$. (d) Changing of power with Δl. (e) $F_x^{l,m}(n)$ with number of kicks at different Δl. Black line represents the exponential decrease of local maxima of saturating amplitude.

In a nutshell, we see that the characteristic regions of LMOTOCs have similar behavior for $\hat{\mathscr{U}}_0$ and $\hat{\mathscr{U}}_x$ systems. In both cases, the commutator propagation varies with τ in a similar way. But the dynamic region displays a contrast between $\hat{\mathscr{U}}_0$ and $\hat{\mathscr{U}}_x$. In the integrable case, the exponent of the power-law increases linearly with Δl, but in the nonintegrable exponent, we see a quadratic growth of power-law with Δl. In the saturation region, both are oscillating, and the envelope decreases with different rates.

In this chapter, we considered single spins as observables in our calculation of OTOCs. The experimental procedure of calculating OTOC using single spin observables and initial product state has been done in Ref. [136]. Implementation of the unitary operator on observable $\hat{W}^l$ $\left[\hat{W}^l(n) = (\hat{\mathscr{U}_x}^\dagger)^n \hat{W}^l(0)(\hat{\mathscr{U}_x})^n\right]$ followed by perturbation of observable $\hat{V}^m$ is discussed in the Ref. [100]. The OTOC is obtained by measuring the expectation value of the observable $(\hat{\mathscr{U}_x}^\dagger)^n \hat{W}^l(0)(\hat{\mathscr{U}_x})^n \hat{V}^m (\hat{\mathscr{U}_x}^\dagger)^n \hat{W}^l(0)(\hat{\mathscr{U}_x})^n \hat{V}^m$ [136]. Therefore, LMOTOCs and TOMOTOCs can be calculated experimentally.

3.5 Conclusion

We studied the behavior of TMOTOC and LMOTOC comprehensively using $\hat{\mathscr{U}}_0$ and $\hat{\mathscr{U}}_x$ systems. We divided LMOTOC and TMOTOC into three distinct regimes: characteristic-time, dynamic-time, and saturation-time regimes.

Characteristic times of TMOTOC and LMOTOC are independent of the integrability of the system. It is also independent of the Floquet period and system size; however, it depends on the separation between the observables. The number of kicks required for the deviation of $\Re[F^{l,m}]$ from unity is equal to the numerical value of the separation between the observables in the case of TMOTOC; however, one extra kick is required in the case of LMOTOC. Behavior of the dynamic region is also independent of the integrability of the system. In both systems, $\hat{\mathscr{U}}_0$ and $\hat{\mathscr{U}}_x$, LMOTOC, and TMOTOC show the power-law growth. There is no signature of Lyapunov exponent. This power-law growth depends on

the separation between the spins and the Floquet period. The rate of change of exponent with respect to the separation between the spins is independent of the integrability of the system in the TMOTOC; however, we see a dependence in the case of LMOTOC. In TMOTOC for both the systems $\hat{\mathscr{U}}_0$, and $\hat{\mathscr{U}}_x$, the exponent varies as a triangular function. In the case of LMOTOC, we see a triangular function with linear increase/decrease for $\hat{\mathscr{U}}_0$ system but a quadratic increase/decrease for $\hat{\mathscr{U}}_x$ system. Saturation region of TMOTOC is different in both systems: $\hat{\mathscr{U}}_0$ system revives back, but $\hat{\mathscr{U}}_x$ system decays linearly. Saturation behavior of LMOTOC shows the oscillating decay with envelop decaying linearly in both systems. Saturation of TMOTOC and LMOTOC are independent of Δl.

In the next chapter, we will calculate OTOCs using contiguous symmetric blocks of spins or random operators localized on these blocks as observables instead of localized spin observables. In the calculation of OTOC, we consider both integrable and nonintegrable Ising spin Floquet systems.